Received: 6 September 2022 | Revised: 19 October 2022 | Accepted: 23 October 2022

DOI: 10.1002/eng2.12594

RESEARCH ARTICLE

Engineering Reports Open Access WILEY

Determination of layer morphology of rough layers in organic light emitting diodes by X-ray reflectivity

Ian Sachs[1] | **Marc Fuhrmann**[1] | **Wim Deferme**[2,3] | **Hildegard Möbius**[1]

[1]Department of Computer Sciences/Micro Systems Technology, University of Applied Sciences Kaiserslautern, Zweibrücken, Germany

[2]Institute for Materials Research (IMO), Hasselt University, Diepenbeek, Belgium

[3]IMEC vzw, Division IMOMEC, Diepenbeek, Belgium

Correspondence
Hildegard Möbius, Department of Computer Sciences/Micro Systems Technology, niversity of Applied Sciences Kaiserslautern, Amerikastraße 1, 66482 Zweibrücken, Germany.
Email: hildegard.moebius@hs-kl.de

Abstract

X-ray reflectivity (XRR) has been proven to be a useful tool to investigate thin layers as well as buried interfaces in stacks built of very thin layers. Nevertheless, x-ray reflectivity measurements are limited by the roughness of the layers and interfaces as the roughness destroys the interference structure, the so-called Kiessig fringes. As investigations of thin layers in organic light emitting devices (OLEDs) are still subject of research and development, the focus of this paper is the investigation of a layer of indium tin oxide (ITO) which serves as transparent anode material in OLEDs. Due to the fabrication process, ITO shows rough surface structures, so-called spikes, hindering the determination of the ITO layer thickness and roughness in XRR measurements. In this paper, it is theoretically and experimentally proven that a smoothing layer on the ITO enables the determination of the buried ITO layer thickness and roughness as well as the density of the spikes. Furthermore, a sputtered aluminum layer (e.g. cathode material) showing spikes in atomic force microscopy covered with a smoothing layer reveals Kiessig fringes allowing the determination of the density of buried spikes. In general, it is shown that a smoothing layer on a rough surface enhances the sensitivity of x-ray reflectivity measurements.

KEYWORDS

AFM, contrast enhancement, ITO spikes, OLED, x-ray reflection

1 | INTRODUCTION

X-ray reflectivity, XRR, has been proven to be a suitable non-destructive method to investigate stacks of very thin buried layers, small changes in interface roughness and layer thickness as well as the investigation of waviness.[1-4] Neuhold et al. proved that x-ray reflectivity is an excellent tool to investigate buried interfaces in organic electronic devices[5] although the interpretation of XRR measurements depends on a large number of parameters such as thickness and roughness and is therefore difficult.[1] Theoretical considerations discuss the influence of roughness in layer stacks[6,7] and demonstrate the impact of the roughness with decreasing thickness of the layers.

Although organic light emitting devices (OLEDs) already successfully entered the market,[8] there is still a need to replace materials or process steps for various reasons.[8,9] The demand for cost reduction, optimization of parameters

to improve the performance and life-time, ideas for novel functionalities as well as still existing problems like the formation of dark spots in OLEDs lead to intensive research and development. Therefore, OLEDs are continuously adapted to new research results. The topics are ranging from the investigation of dark spots due to pinholes,[10] oxidation of the aluminum cathode,[10,11] the replacement of process steps for various reasons such as changing the deposition technique from spin coating to ultrasonic spray coating,[12,13] and the investigation of spikes of the indium tin oxide layer (ITO).[10] The spikes may cause dark spots due to locally higher electric fields and an overall higher driving voltage of the device.[14] The trend goes toward decreasing layer thickness in OLEDs to increase their efficacy.[15-17] This leads to an increasing importance of the roughness of layers and interfaces of next-generation devices.

In this paper, the focus lies on the investigation of a rough ITO layer to develop and demonstrate a new method to visualize rough layers and spikes in XRR. It is theoretical shown and experimentally proven, that adding a smoothing layer on a rough surface leads to contrast enhancement in the x-ray reflectivity measurement. As ideal candidates to prove this theoretical hypothesis in this paper, sputtered ITO layers and sputtered aluminum layers were chosen. The large spikes form a rough layer destroying the interference signal in x-ray reflectivity, the so-called Kiessig fringes, in measurements of ITO on glass and reducing the amplitude of Kiessig fringes in measurements of aluminum on a silicon substrate. The results show that in general the layer thickness of layers with surfaces too rough to create Kiessig fringes can be determined by filling the rough surface with a material of different electron density. In this case, Kiessig fringes appear due to the thickness of the second layer as well as of the layer with the rough surface resulting from an intermediate layer with an electron density between the electron density of the first (rough) layer and the second layer. Thus, the layer thickness of the rough layer as well as the spike density can now be determined. Generally spoken, the new approach using a smoothing layer to cover a rough layer enhances the resolution in XRR measurements.

2 | MATERIALS AND METHODS

For the experimental section, the following monolayer and multilayer systems were used (Table 1). For our investigations, we used layers and materials typically used in organic light emitting diodes. We use parts of a typical OLED stack with float glass as substrate, indium tin oxide (ITO, CEC010S, Präzisions Glas & Optik GmbH) as anode material and super yellow (SY) as emitter as well as aluminum as cathode material.

2.1 | X-ray reflectivity

XRR measurements were performed with Bruker D8 diffractometer (Bruker Cooperation) using Copper K_α radiation with a wavelength of $\lambda = 0.154059$ nm. The detector filter consists of Nickel (K_β Filter). The slits for the tube and detector were set to 0.1 and 0.2 mm and for the probe slit at 50 µm. The increments were set to 0.001° with a scan time from 1 to 120 s. The software used for the simulation and calculation is Bruker DIFFRACplus LEPTOS v6.

TABLE 1 Materials and thickness used in layer stacks for x-ray reflectivity experiments

Layer	Material	Thickness
Substrate	Float glass[a]	1.1 mm
Anode	Indium tin oxide[a]	180 nm
Emitter	Super yellow[b]	30–60 nm
Cathode	Aluminum	100 nm

[a] https://www.pgo-online.com/de/ito.html-CEC010S.
[b] https://www.sigmaaldrich.com/DE/en/product/aldrich/900438.

2.2 | AFM

The AFM measurements of the topography were performed using the Bruker Dimension I AFM (Bruker Corporation) in tapping mode. The AFM tip used is a SSS-MFMR tip with a radius of r = 15 nm. The scan size was 10 μm with 128 lines using 256 samples/line and a scan rate of 0.996 Hz.

2.3 | Sample preparation

The Si substrates were cut from a silicon wafer (Siegert Wafer GmbH. *n*-type, one side polish, diameter $d = 100$ mm) into 25×25 mm^2 squares. To avoid defects in the surface, the backside of the substrates was used, which was glued and protected on the carrier film for cutting. Subsequently, the substrates were cleaned (DI water) and treated in the reactive ion etching system (Sentech Instruments GmbH) in an oxygen plasma (45%, 100 W, 10 min). The plasma strips organic residues on the surface and also activates the surface. A glovebox with a nitrogen atmosphere was used to apply the coating systems. These organic light emitting materials are susceptible to oxygen and water vapor in the air and oxidize in normal atmosphere.

The organic polymer super yellow was spin coated onto the substrate. For this purpose, it was dissolved in anisole. After spin coating, the samples were baked on a hotplate for 15 min at 90°C.

For the ITO layer, purchased substrates (CEC010S, Präzisions Glas & Optik GmbH) were used. These consist of float glass with a sputtered ITO layer (10 ohm/sq) and a nominal thickness of $d = 180$ nm. The substrates were cleaned and treated in oxygen plasma according to the glass substrates. In addition, topography and roughness of the substrates were studied with the AFM (Bruker Corporation).

All samples were baked (90°C, 10–12 min) on a hot plate in the intermediate steps to drive out solvent. A profilometer was used to check the layer thicknesses (Dektak XT, Bruker Corporation).

The aluminum samples were sputtered onto the polished side of a cut silicon wafer (25×25 mm^2, Siegert Wafer GmbH. n-type, one side polish, diameter $d = 100$ mm) using a SenVac Anlagen & Komponenten GmbH sputter machine Z590 (1 min etch, 600 W, DC; 3 min sputter, 1500 W, HF). The time parameter was adjusted to a layer thickness of approximately $d = 100$ nm.

3 | THEORY

Contrast in x-ray reflectivity is due to variation of the refractive index and thus electron density variations perpendicular to the substrate:

$$n = 1 - \delta, \tag{1}$$

$$\delta = \frac{r_e \rho \lambda^2}{2\pi}, \tag{2}$$

where n is the refractive index, r_e is electron radius, λ is wavelength of the x-rays, and ρ is electron density of the material.

The calculation of x-ray reflectivity curves is based on a Fourier transform technique[4,18] leading to the following reflectivity

$$R(\mathrm{q}) = \left| \frac{8\pi^2}{\lambda^2 \mathrm{q}} \int_{-\infty}^{+\infty} \delta(\mathrm{z}) e^{i q_z z}\, dz \right|^2, \tag{3}$$

with

$$\mathrm{q} = \frac{4\pi \sin\theta}{\lambda}, \tag{4}$$

and

$$\delta(z) = \frac{r_e \lambda^2}{2\pi} \rho(z), \tag{5}$$

where θ is incidence angle, z is direction perpendicular to the surface, and $\rho(z)$ is electron density as a function of z clearly indicating that electron density variations determine the reflectivity curve.

Measuring the substrate only the interface substrate—air contributes to the reflectivity curve due to the change of electron density at the surface resulting in a smooth curve. Measuring instead a thin film on the substrate, an additional interface in form of a jump of electron density occurs leading to so-called Kiessig fringes (Figure 1A). The Kiessig fringes result from interference of reflected beams at the two interfaces and are therefore very sensitive to the layer thickness and the roughness of the layer. Adding more layers in the stack, more interfaces and therefore more interference effects occur and are superimposed (Figure 1E).

4 | RESULTS AND DISCUSSION

4.1 | Simulation

If the roughness of a layer exceeds a certain value, the Kiessig fringes disappear and there is no possibility to determine the layer thickness from the reflectivity curve (Figure 1C,D). The roughness is defined according to Névot et al., who approximated the rough interface by a Gaussian distribution.[19,20] However, theoretical considerations predict that adding a smoothing layer (layer 2) on the rough surface (of layer 1) the contrast can be enhanced so that the determination of the thickness of the rough layer is possible (Figure 1E,F). Adding a smoothing layer on the rough surface can be modeled by an additional intermediate layer (IML) between layer 1 and layer 2 with an electron density between the electron density of the material with the rough surface and the material used as a smoothing layer (Figure 2). In this model calculation, the first layer now has a low roughness as the actual roughness contributes to the IML in form of an averaged electron density of the materials of layer 1 and layer 2.

This IML consists of a volumetric mixture of both materials (rough and smoothing layer) with a density defined by the volumetric ratio of the two materials. The reflectivity curve now shows Kiessig fringes corresponding to both layers as shown in Figure 1E. Figure 1A,C shows the typical reflectivity curve for a smooth (roughness <1 nm) and a rough layer (roughness >5 nm) on glass. Figure 1B,D shows the density profiles of the layers. High roughness values lead to broadened interfaces. Adding an IML (volume fraction of 50% rough layer and 50% smoothing layer, d(IML) = 20 nm) leads to Kiessig fringes corresponding to the smooth and the rough layer (Figure 1E).

Thus, a smoothing layer with a lower electron density than the rough layer allows to determine thickness and roughness of the rough layer as well. Additionally, the electron density of the IML and the volume fraction of both materials in the intermediate layer can be determined.

4.2 | Experimental

ITO used in typical OLED stack as a transparent anode is an ideal candidate to test the new approach of using a smoothing layer to enhance the sensitivity of the XRR measurements. ITO is sputtered onto the glass with a thickness of approx. 180 nm (CEC010S) and a high roughness (approximately 5 nm determined by AFM). In addition, the sputtering process produces spikes with a height of 20–30 nm (Figure 4). The measurements of an ITO layer on float glass do not show Kiessig fringes (Figure 3) due to the high roughness of the ITO.

Thus, the thickness of the ITO layer cannot be determined from the XRR measurement. AFM measurements of the ITO layer confirm a large roughness value due to spikes (Figure 4):

Figure 4A,B shows the AFM topography measurements in 3D and 2D to visualize the surface structure. The sample shows a maximum spike height of 31 nm spikes with a roughness of R_a = 4.9 nm determined by AFM. Figure 3C shows

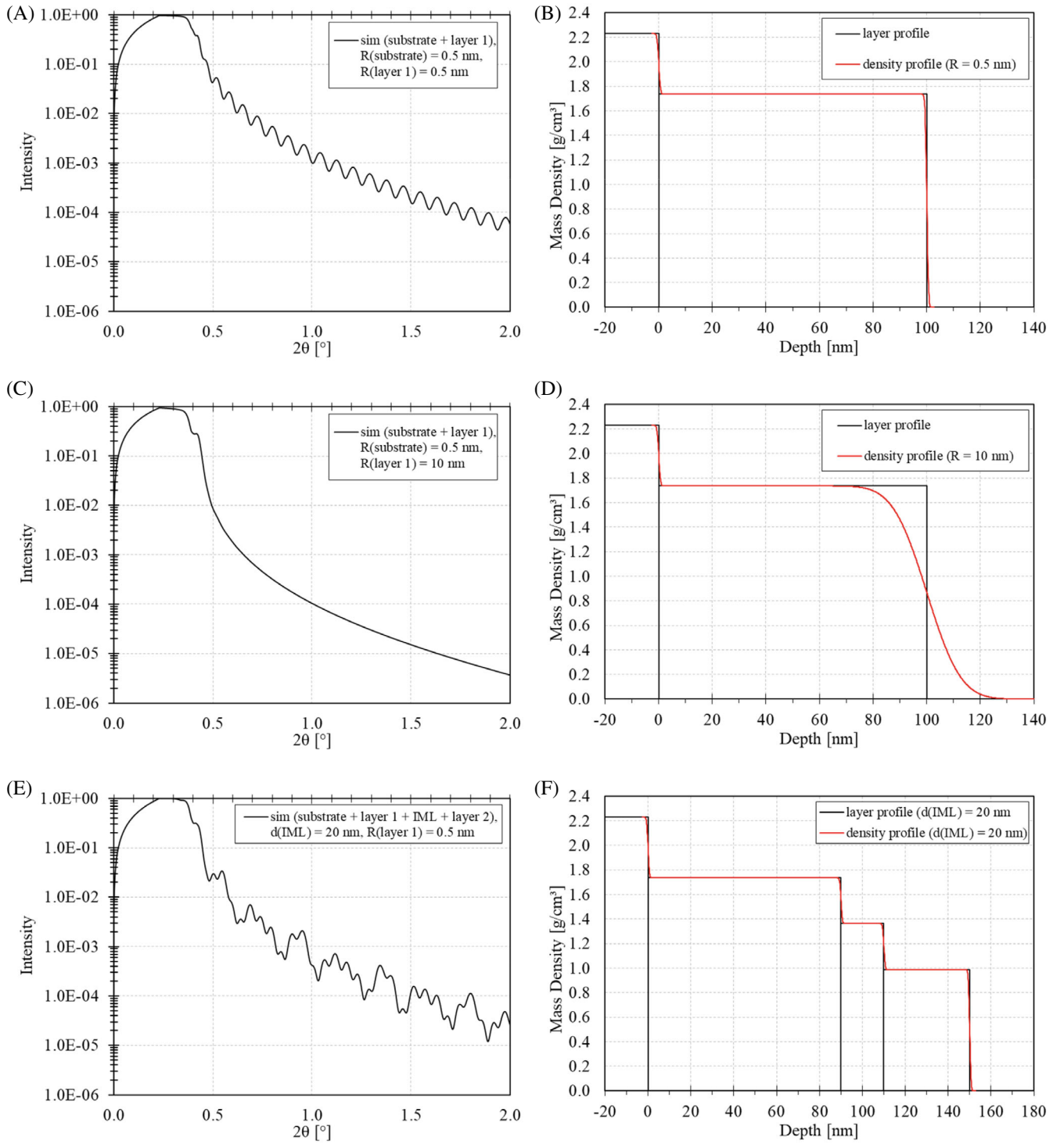

FIGURE 1 (A) Calculated curve for glass and a thin layer (layer 1) with an electron density smaller than the electron density of glass with low roughness (R(substrate) = 0.5 nm; R(layer 1) = 0.5 nm). (B) Density profile for (A). (C) Calculated curve for glass and layer 1 with high roughness of layer (R(substrate) = 0.5 nm; R(layer 1) = 10 nm) canceling Kiessig fringes. (D) Density profile for (C). (E) Calculated curve including IML (volume fraction of 50% rough layer and 50% smoothing layer). (F) Density profile for (E)

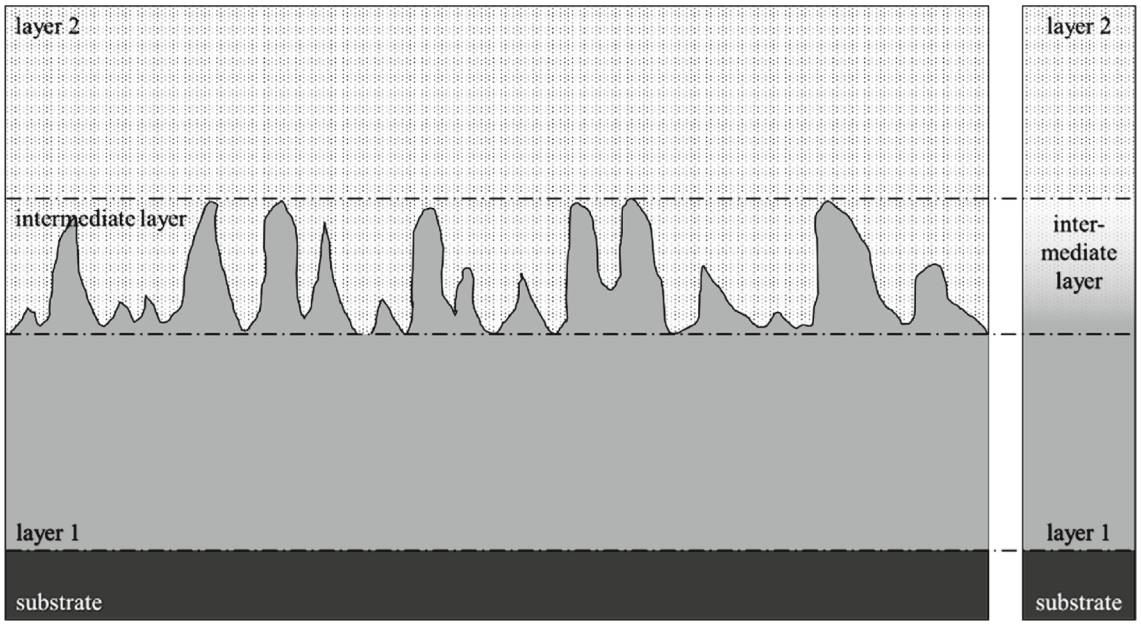

FIGURE 2 Layer stack with rough surface and smoothing layer creating an intermediate layer. Right side demonstrates the blend of the layers according their color and pattern.

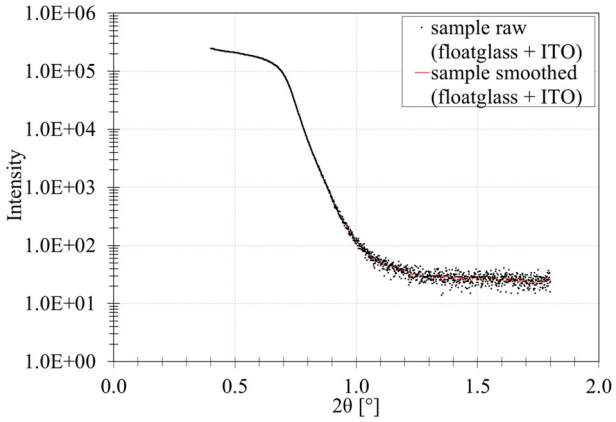

FIGURE 3 Indium tin oxide on glass substrate with smoothed measurement. No Kiessig fringes visible

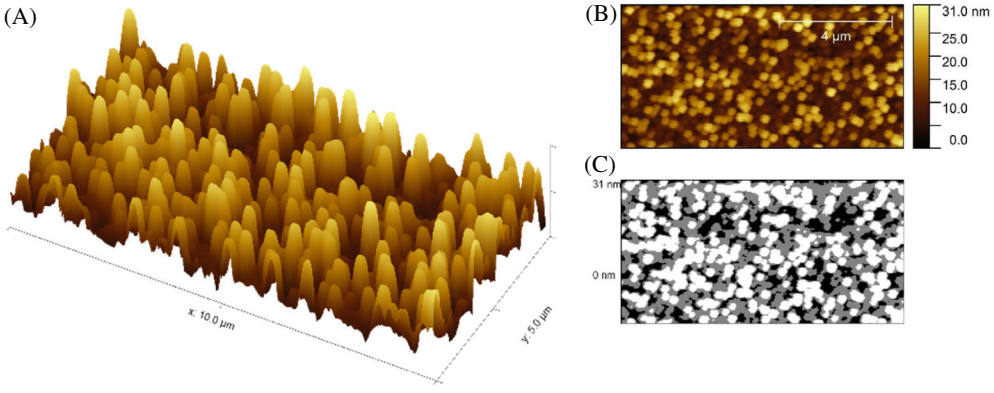

FIGURE 4 (A) Three-dimensional AFM image of indium tin oxide (ITO) spikes on floatglass substrate. (B) Topography measurement (AFM) of ITO layer on floatglass substrate. (C) Calculation of spike percentage of the ITO layer: black <10 nm (22.3%), gray <20 nm (44.1%) and white up to maximum of 31 nm (33.6%).

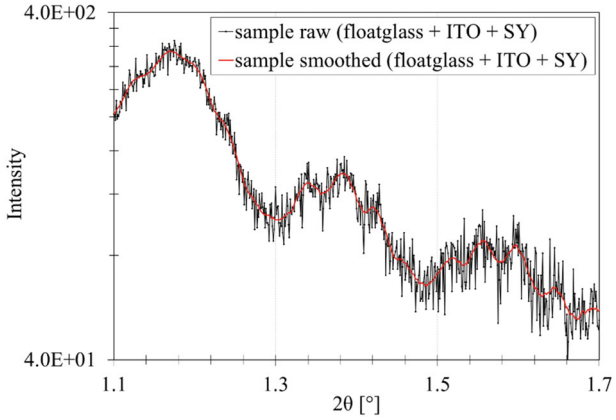

FIGURE 5 Measurement of glass, indium tin oxide and super yellow sample with reappearing Kiessig fringes with smoothed curve (red) to clarify Kiessig fringes

the number of spikes by greyscale: dark spots represent heights lower than 10 nm. Gray and white spots show spikes up to 20 nm and spikes larger than 20 nm, respectively. Their volumetric portion can be calculated by the topography image. The large spikes (20–31 nm) depict a volume fraction of approx. 33.6%, the medium spikes (10–20 nm) of 44.1% and small spikes (<10 nm) of 22.3%. The spikes form a dense packed structure. So, it is likely that the spin coated SY layer only fills 5–10 nm of the upper part of the structure, the volume between the top of the medium spikes and the top of the large spikes. The volume fraction of the spikes in this upper layer is approximately two-third of the total volume.

As shown in the simulations above, theory predicts that using a smoothing layer (super yellow, AFM roughness R_q = 0.74 nm), it is possible to visualize and calculate the layer thickness of a layer with roughness too high to reveal Kiessig fringes in XRR for this layer on a smooth substrate. In order to prove theory in this work, ITO layers were covered by a thin film of SY as a smoothing layer. Kiessig fringes corresponding to the layer thickness of the SY layer appear as well as Kiessig fringes corresponding to the layer thickness of the ITO-layer (Figure 5).

The fits in Figure 6A,B reveal an IML with an electron density between the electron density of the ITO layer and the electron density of the SY layer (Table 2). It is even possible to determine the volume fraction of the ITO (spikes) in the IML. By fitting the electron density of the IML, the volume fraction of the spikes is determined to be approximately 70%. This value is in accordance with the volume fraction of the spikes determined by the AFM measurements (approximately 66.4%).

The roughness of the ITO layer can be determined by the thickness of the modeled IML. The fitted thickness of the IML of d = 5.4 nm corresponds to the actual surface roughness of ITO and is in accordance with the AFM measurements (Figure 4).

To confirm the measurements, a different stack of material using Si, Al and super yellow, SY, was prepared. To gain a similar rough surface as ITO, the aluminum layer was sputtered onto the substrate with a thickness of approximately 100 nm. As aluminum will create a native oxide layer (Al_2O_3) approximately 4-nm thick,[11] the oxide film will be added to the layer stack for calculations. Before adding the SY layer, the Si Al stack was investigated by using AFM as shown in Figure 7.

The roughness of the AFM measurement represents the roughness of the thin oxide layer with approx. R_q = 4.7 nm. As in ITO substrates, the AFM measurements reveal the existence of spikes due to the sputtering process. However, the spikes differ in their appearance compared to the ITO spikes: their height is larger than the ITO spikes with up to 56 nm, while their lateral size is smaller and in the range of 130 nm diameter (ITO: approximately 400 nm diameter).

XRR measurements (Figure 8) show weak Kiessig fringes corresponding to the large roughness (Table 3) determined by the AFM measurements (Figure 7). The Al thickness matches the prediction of the sputtering time (see sample preparation).

By adding SY by spin coating on top of the Al layer, the Kiessig fringes are much more pronounced indicating a lower roughness (Table 4) in the system (Figure 9A,B). Additionally, a further frequency appears in the Kiessig fringes (Figure 9A,B) due to an additional layer with low roughness. Simulations (Figure 9C) show that this cannot be explained

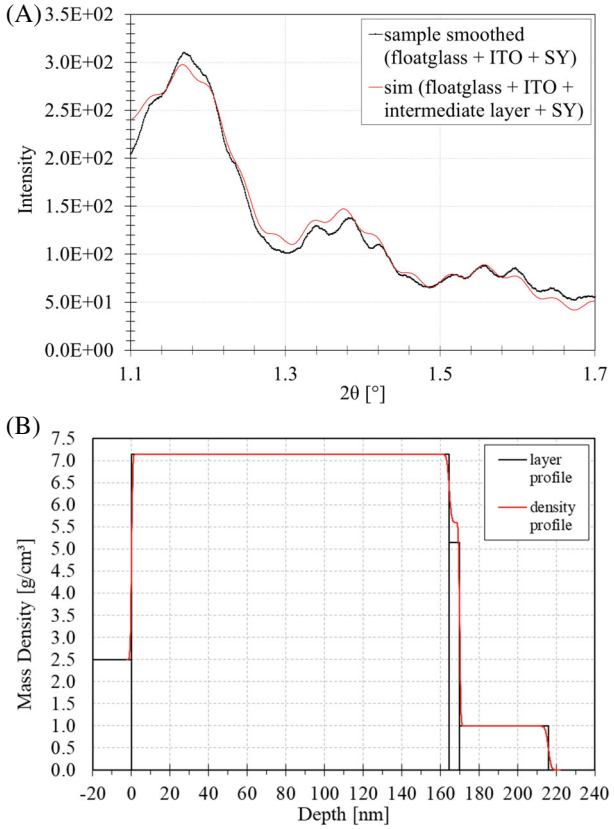

FIGURE 6 (A) Measurements from Figure 5 with calculated curve (red) for thickness determination using intermediate layer (70% of indium tin oxide). (B) Density profile of the sample used for the fit

TABLE 2 Layer thickness and roughness for calculation in Figure 6

Layer	Roughness *R* (nm)	Thickness *d*
floatglass	0.50	Bulk
ITO	0.96	164.5 nm
Intermediate layer (70% ITO)	0.50	5.400 nm
Super yellow	1.18	45.90 nm

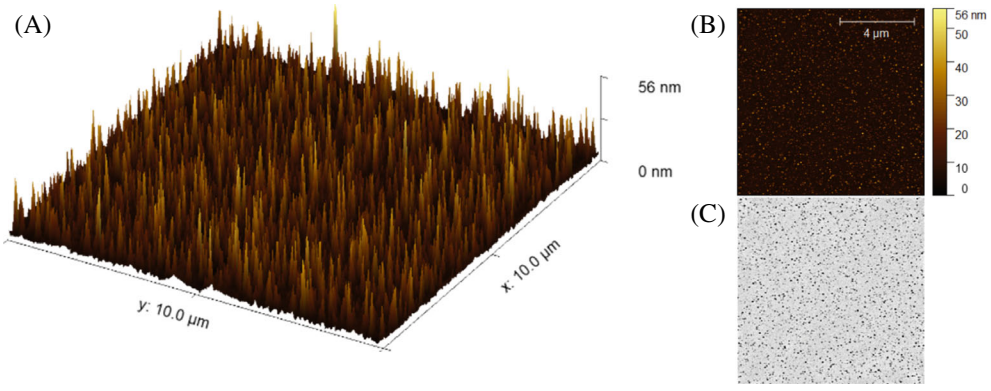

FIGURE 7 (A) Three-dimensional AFM image of spikes on Si Al stack. (B) Topography measurement (AFM) of spikes on Si Al stack. (C) Calculation of spike percentage of the indium tin oxide layer: black <56 nm (24.9%) and gray <25 nm (12.4%)

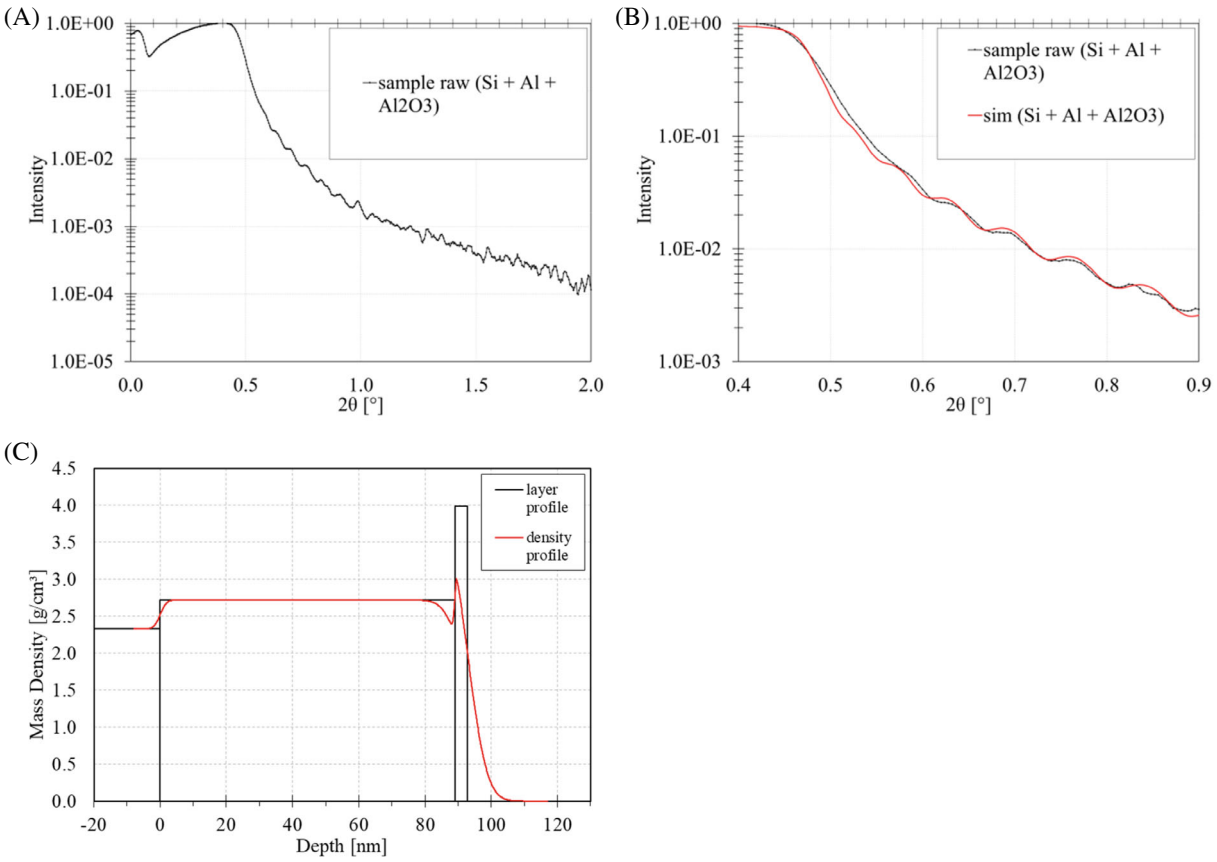

FIGURE 8 (A) X-ray reflectivity measurement of Si Al stack showing low intensity of fringes. (B) Measurement (black) and calculated curve (red) for Si Al stack. (C) Density profile for (B)

TABLE 3 Layer thickness and roughness for calculation in Figure 8

Layer	Roughness *R* (nm)	Thickness *d*
Si	1.5	
Al	0.5	89 nm
Al2O3	4.6	3.8 nm

TABLE 4 Layer thickness and roughness for calculation in Figure 9, (A) for Figure 9C and (B) for Figure 9D

(A)		
Layer	**Roughness *R* (nm)**	**Thickness *d***
Si	1.5	
Al	0.5	89
Al_2O_3	4.6	3.8
SY	0.5	74
(B)		
Layer	**Roughness *R* (nm)**	**Thickness *d***
Si	1.5	
Al	0.5	89
Al_2O_3	1.5	3.8
IML	0.5	69.5
SY	0.5	42.5

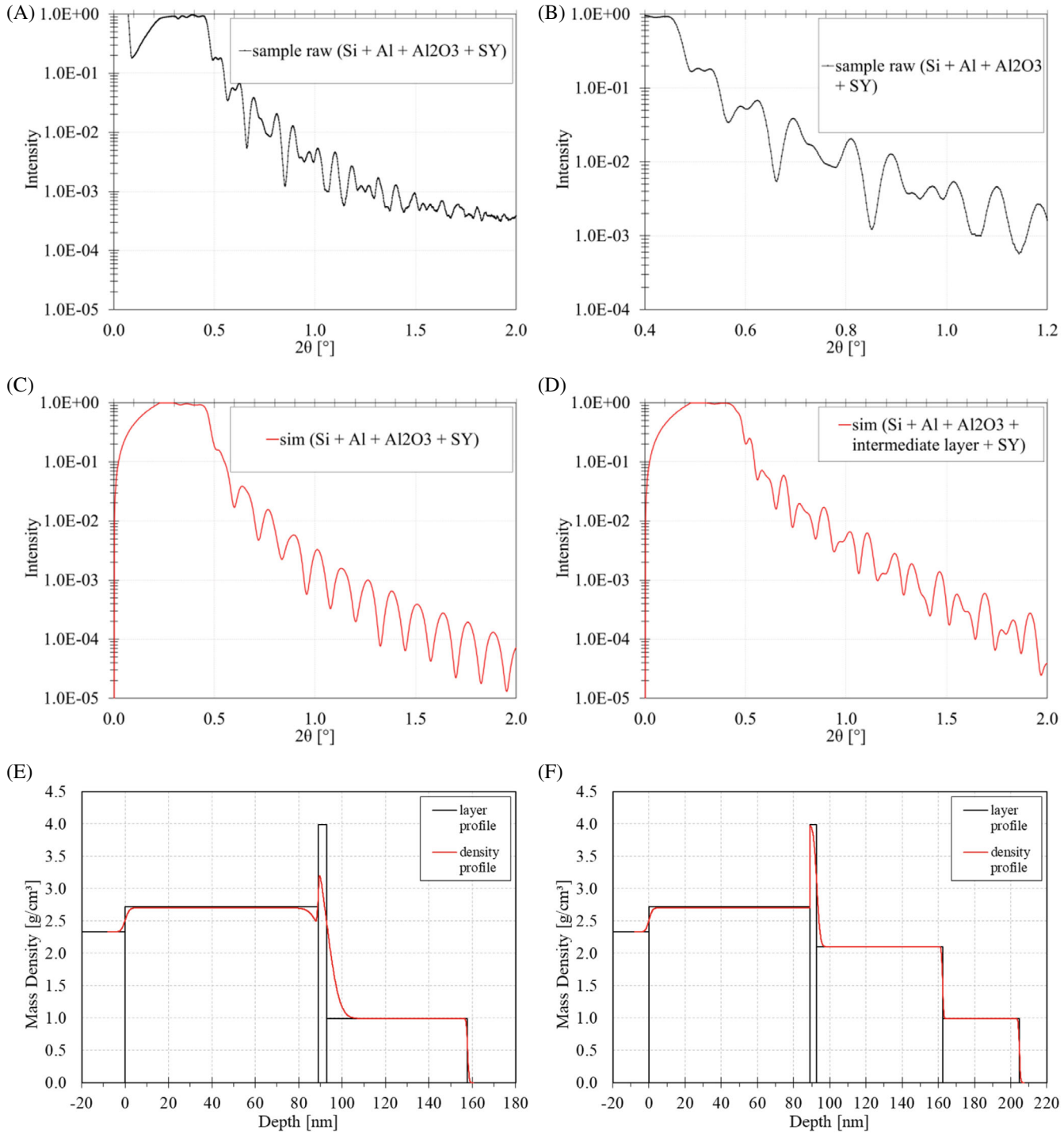

FIGURE 9 (A) Measurement of multilayer stack (Si, Al, Al_2O_3, super yellow) in the range of $2\theta = 0–2.0°$. (B) Zoomed in measurement of (A) in the range of $2\theta = 0.4–1.2°$. (C) Calculated curve for the multilayer stack (Si, Al, Al_2O_3, super yellow) using the measured parameters by AFM (thickness and roughness). (D) Calculated curve using an intermediate layer to compensate the spikes of the Al surface. (E) Density profile for (C). (F) Density profile for (D)

TABLE 5 Layer thickness and roughness for calculation in Figure 10

Layer	Roughness *R* (nm)	Thickness *d*
Si	1.5	
Al	0.5	84
Al_2O_3	2.6	3.5
Intermediate layer	0.3	78.7
SY	0.5	45

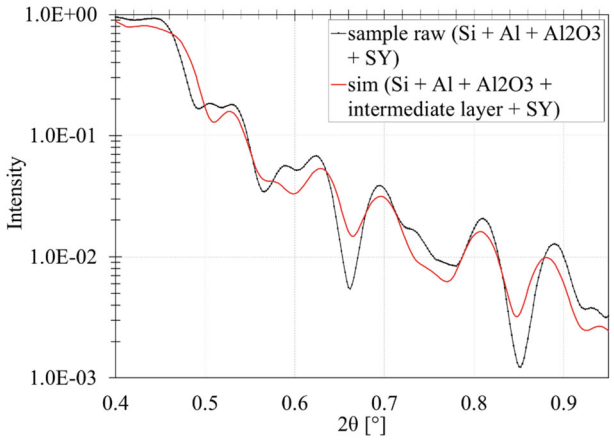

FIGURE 10 Fit of the measurement by assuming an intermediate layer composed of spikes and SY.

by simply adding a SY layer in the simulations according to the expected SY layer thickness (Figure 9A,C) but the measurements suggest again the existence of an IML between the Al layer and the SY layer, consisting of the Al spikes filled with SY material (Figure 9D). For this simulation, the layer thickness of the Al layer is determined by the XRR measurement of the Al layer (Figure 8), the thickness of the IML by using the height of the spikes by AFM measurements and the height of the remaining SY layer by estimating the SY material left after filling the spikes with SY. The spike density of approx. 25% was determined by the AFM measurements.

In contrast to the measurements using ITO as a substrate for SY, the spikes on the Al substrates show a different shape and size. The spikes have a similar height but a much smaller diameter and are more isolated. For this reason, the IML differs in its size and composition from the ITO simulation. As the SY layer is spin coated onto the Al substrate, SY might not fil all spaces between the spikes. Nevertheless, it is possible to fit the measurement data by using the thickness of the IML and the thickness of the SY layer as fitting parameters (Table 5) shown in Figure 10.

Thus, the measurements and simulations confirm the theory that adding a smoothing layer to a rough layer allows the determination of the morphology of rough buried layers.

5 | CONCLUSION

In this paper, a new method is developed to visualize rough surfaces in x-ray reflectivity by using a smoothing layer on top of the rough surface. The smoothing layer leads to an IML between the rough layer and the smoothing material with a value of the electron density between the value of the electron densities of the rough layer and the smoothing layer. It is theoretically calculated and demonstrated that for this system Kiessig–Fringes appear allowing the determination of the thickness and roughness of the rough layer as well. ITO layers and Al layers in OLED stacks are used to experimentally prove theory and to determine the spike density in buried layers.

AUTHOR CONTRIBUTIONS

Hildegard Möbius: Conceptualization (lead); formal analysis (supporting); methodology (equal); project administration (lead); resources (lead); validation (lead); writing – review and editing (lead). **Ian Sachs:** Conceptualization (supporting); data curation (equal); formal analysis (supporting); investigation (lead); methodology (equal); project administration (supporting); resources (lead); validation (lead); writing – original draft (lead); writing – review and editing (equal). **Marc Fuhrmann:** Data curation (supporting); investigation (supporting); writing – review and editing (supporting). **Wim Deferme:** Conceptualization (lead); project administration (equal); resources (equal); supervision (lead); validation (equal); writing – review and editing (equal).

CONFLICT OF INTEREST

Authors have no conflict of interest relevant to this article.

PEER REVIEW

The peer review history for this article is available at https://publons.com/publon/10.1002/eng2.12594.

DATA AVAILABILITY STATEMENT

The data that support the findings of this study are available from the corresponding author upon reasonable request.

ACKNOWLEDGMENT

Open Access funding enabled and organized by Projekt DEAL.

ORCID

Ian Sachs https://orcid.org/0000-0001-5023-9587
Marc Fuhrmann https://orcid.org/0000-0002-1030-6578
Wim Deferme https://orcid.org/0000-0002-8982-959X
Hildegard Möbius https://orcid.org/0000-0003-2725-9752

REFERENCES

1. Spiga D, Mirone A, Pareschi G, et al. Space telescopes and instrumentation II: ultraviolet to gamma rayin. In: Turner MJL, Hasinger G, eds. *Space Telescopes and Instrumentation II: Ultraviolet to Gamma Ray*. SPIE; 2006:626616.
2. Hu N, Dong X, He X, Browning JF, Schaefer DW. Effect of sealing on the morphology of anodized aluminum oxide. *Corros Sci*. 2015;97:17-24.
3. Colombi P, Agnihotri DK, Asadchikov VE, et al. Reproducibility in X-ray reflectometry: results from the first world-wide round-robin experiment. *J Appl Cryst*. 2008;41:143-152.
4. Mensinger H, Stamm M, Boeffel C. Order in thin films of a liquid crystalline polymer. *J Chem Phys*. 1992;96:3183-3190.
5. Neuhold A, Brandner H, Ausserlechner SJ, et al. X-ray based tools for the investigation of buried interfaces in organic electronic devices. *Organ Electron*. 2013;14:479-487.
6. Fujii Y. Recent developments in the X-ray reflectivity analysis for rough surfaces and interfaces of multilayered thin film materials. *J Mater*. 2013;2013:1-20.
7. Esashi Y, Tanksalvala M, Zhang Z, Jenkins NW, Kapteyn HC, Murnane MM. Influence of surface and interface roughness on X-ray and extreme ultraviolet reflectance: a comparative numerical study. *OSA Contin*. 2021;4:1497.
8. Hong G, Gan X, Leonhardt C, et al. A brief history of OLEDs—emitter development and industry milestones. *Adv Mater*. 2021;33:2005630.
9. Sachs I, Fuhrmann M, Verboven I, Basak I, Deferme W, Möbius H. Inkjet-printed lenses with adjustable contact angle to improve the light out-coupling of organic light-emitting diodes. *Adv Eng Mater*. 2021;23:2100212.
10. Azrain MM, Mansor MR, Fadzullah S, et al. Analysis of mechanisms responsible for the formation of dark spots in organic light emitting diodes (OLEDs): a review. *Synth Met*. 2018;235:160-175.
11. Evertsson J, Bertram F, Zhang F, et al. The thickness of native oxides on aluminum alloys and single crystals. *Appl Surf Sci*. 2015;349:826-832.
12. Verboven I, Silvano J, Elen K, et al. Ultrasonic spray coating of silver nanowire-based electrodes for organic light-emitting diodes, *Adv Eng Mater* 2021;24:2100808.
13. Gilissen K, Stryckers J, Verstappen P, et al. Ultrasonic spray coating as deposition technique for the light-emitting layer in polymer LEDs. *Organ Electron*. 2015;20:31-35.
14. Liu G, Kerr JB, Johnson S. Dark spot formation relative to ITO surface roughness for polyfluorene devices. *Synth Met*. 2004;144:1-6.
15. Kim E, Kwon J, Kim C, Kim T-S, Choi KC, Yoo S. Design of ultrathin OLEDs having oxide-based transparent electrodes and encapsulation with sub-mm bending radius. *Organ Electron*. 2020;82:105704.

16. Kang SW, Baek D-H, Ju B-K, Park YW. Green phosphorescent organic light-emitting diode exhibiting highest external quantum efficiency with ultra-thin undoped emission layer. *Sci Rep*. 2021;11:8436.
17. Nanda GP, Sk B, Yadav N, et al. Ultrathin non-doped thermally activated delayed fluorescence emitting layer for highly efficient OLEDs. *Chem Commun*. 2021;57:13728-13731.
18. Bridou F, Pardo B. Use of Fourier transfoim in grazing X-rays reflectometry. *J Phys III*. 1994;4:1523-1531.
19. Névot L, Croce P. Caractérisation des surfaces par réflexion rasante de rayons X. Application à l'étude du polissage de quelques verres silicates. *Rev Phys Appl*. 1980;15:761-779.
20. Filies O, Böling O, Grewer K, et al. Surface roughness of thin layers—A comparison of XRR and SFM measurements. *Appl Surf Sci*. 1999;141:357-365.

How to cite this article: Sachs I, Fuhrmann M, Deferme W, Möbius H. Determination of layer morphology of rough layers in organic light emitting diodes by X-ray reflectivity. *Engineering Reports*. 2023;5(4):e12594. doi: 10.1002/eng2.12594